

A NEW, SOFT-SWITCHED BOOST CONVERTER WITH ISOLATED ACTIVE SNUBBER

Milan M. Jovanović and Yungtaek Jang

DELTA Power Electronics Lab., Inc.
1872 Pratt Drive, Suite 1400
Blacksburg, VA 24060

Abstract - A boost converter which employs an isolated active snubber to reduce the losses caused by the reverse-recovery characteristic of the boost rectifier and the turn-on discharge loss of the output capacitance of the boost switch is described. The proposed isolated active snubber consists of a coupled inductor, clamp capacitor, and ground-referenced N-type MOSFET. The performance of the proposed converter is evaluated on an 1-kW, universal-line-range, boost input-current shaper.

I. Introduction

Generally, at higher power levels, the continuous-conduction-mode boost converter is the preferred topology for implementing the front-end converter for active input-current shaping. The output voltage of the boost input-current shaper is relatively high since the dc-output voltage of the boost converter must be higher than the peak input voltage. Due to the high output voltage, the converter requires the use of a fast-recovery boost rectifier. At high switching frequencies, fast-recovery rectifiers produce significant reverse-recovery-related losses when switched under “hard” switching conditions [1]. These losses can be significantly reduced and, therefore, a high efficiency can be maintained even at high switching frequencies by employing a soft-switching technique.

So far, a number of soft-switched boost converters and their variations have been proposed [2] - [7]. All of them employ an auxiliary active switch with a few passive components (inductors and capacitors) to form an active snubber [8] that is used to control the di/dt rate of the rectifier current and to create conditions for zero-voltage switching (ZVS) of the main switch and the rectifier.

The boost converter circuits proposed in [2] - [4] use a snubber inductor connected to the common node of the boost switch and the rectifier to control the rectifier di/dt. As a result of the snubber-inductor location, the main switch and rectifier in the circuits proposed in [2] - [4] possess the minimum voltage and current stresses. In addition, the boost switch turns on, and the rectifier turns off under zero-voltage (soft-switching) conditions. However, the auxiliary switch turns on while its voltage is equal to the output voltage, and

subsequently turns off while carrying a current greater than the input current, *i.e.*, it operates under “hard” switching conditions.

In the circuits introduced in [5] - [7], the di/dt rate of the rectifier current is controlled by a snubber inductor connected in series with the boost switch and rectifier. Because of the inductor placement, the voltage stress of the main switch is higher than that of the circuits described in [2] - [4]. This increased voltage stress can be minimized by a proper selection of the snubber-inductance value and the switching frequency [7]. Both the boost and the auxiliary switches in the circuits in [5] - [7] operate under ZVS conditions.

The major deficiency of the boost converters described in [2] - [4] is a severe, undesirable resonance between the output capacitance of the auxiliary switch, C_{oss} , and the resonant inductor, which occurs after the auxiliary switch is open and the snubber-inductor current falls to zero. This resonance adversely affects the operation of the circuit and must be eliminated. For example, in the circuit introduced in [3], the resonance is eliminated by the addition of a rectifier and a saturable inductor in series with the snubber inductor, which degrades the conversion efficiency and increases the component count and cost of the circuit.

The circuits described in [5] - [7] also suffer from a number of deficiencies. The common drawback of these circuits is that they require either isolated (high-side) gate drive, if the auxiliary switch is an N-channel MOSFET, or the employment of a P-channel MOSFET, if a non-isolated (direct, low-side) drive is to be used. Both the implementation with an isolated gate drive and the implementation with a P-channel MOSFET are less desirable than the implementation with a non-isolated gate drive and an N-channel MOSFET due to the increased circuit complexity and cost. Also, the circuits introduced in [6] and [7] require a precise and noise-robust gate-drive timing since accidental overlapping of the main and auxiliary switch gate drives may lead to a fatal circuit failure due to a relatively large transient current through the series connection of the simultaneously-conducting main and auxiliary switches. The circuit introduced in [5] does not suffer from the overlapping gate-drive problem because it actually requires an overlapping gate drive for a proper operation. Finally, the circuit in [6] suffers from yet another major drawback caused by the parasitic

resonance between the junction capacitance of the rectifier and the snubber inductor, which significantly increases the voltage stress of the rectifier. As a result, implementation in [6] requires a rectifier with a higher voltage rating, which further increases the cost of the circuit and reduces its conversion efficiency.

In this paper, a technique which improves the performance of the boost circuit using the same approach as in [5] - [7] but employs only N-channel MOSFETs is presented. This technique reduces the reverse-recovery-related losses by controlling the di/dt rate of the rectifier current with a coupled-inductor snubber whose primary winding is connected in series with the boost switch and rectifier. In addition, the energy stored in this coupled inductor is used to discharge the output capacitance of the boost switch to zero prior to the switch turn-on, thus eliminating its capacitive turn-on switching loss. The series connection of the auxiliary switch and the clamp capacitor, which is used to provide the discharging path of the snubber inductor current (energy) when the main switch is turned off, is connected to the output through the secondary winding of the snubber inductor. Because in this circuit arrangement the main and auxiliary switches are not connected in series, the converter is not susceptible to failures due to the accidental, transient overlapping of the main and auxiliary switch gate drives. The technique described in this paper using the boost converter topology can be extended to any other non-isolated or isolated converter topology.

II. Principle of Operation

The circuit diagram of the boost converter which employs the isolated active snubber for reverse-recovery-loss reduction is shown in Fig. 1. The circuit in Fig. 1 uses a coupled-inductor snubber, whose primary winding N_1 is connected in series with the boost switch and rectifier, to control the di/dt rate of the rectifier when boost switch S is turned on. In addition, the series connection of ground-referenced, N-channel-MOSFET auxiliary switch S_1 , clamp capacitor C_C , and secondary winding N_2 of the coupled inductor is used to discharge the energy stored in the inductor

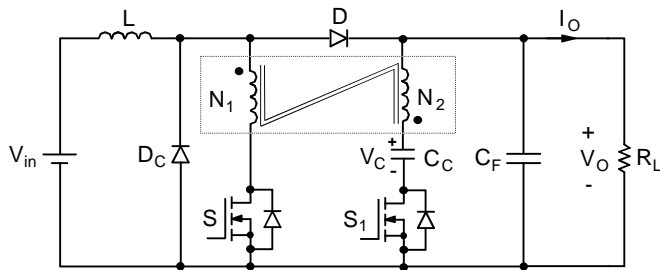


Fig. 1 Boost power stage with isolated active snubber.

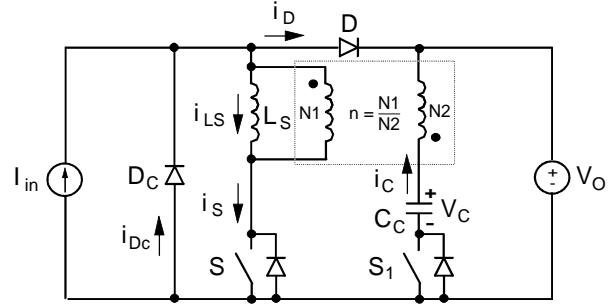


Fig. 2 Simplified circuit diagram of the proposed boost power stage showing reference directions of currents and voltages.

to the output after S_1 is turned off. Diode D_C is employed to eliminate the parasitic ringing between the junction capacitance C_D of rectifier D and the snubber inductor by clamping the anode of D to ground.

To simplify the analysis of operation, it is assumed that the inductance of boost inductor L is large so that it can be represented by constant-current source I_{in} , and that the output-ripple voltage is negligible so that the voltage across the output filter capacitor can be represented by constant-voltage source V_O . Also, it is assumed that in the on-state, semiconductors exhibit zero resistances, *i.e.*, they are short circuits. However, the output capacitance of the MOSFETs and the reverse-recovery charge of the rectifier are not neglected in this analysis. The circuit diagram of the simplified converter is shown in Fig. 2. As can be seen from Fig. 2, for the sake of analysis, the coupled inductor is modeled with the magnetizing inductance L_S and the ideal transformer which has a turns ratio of $n = N_1 / N_2$, where N_1 and N_2 are the numbers of turns of the coupled inductor's primary and secondary windings, respectively.

To further facilitate the explanation of operation, Fig. 3 shows the topological stages of the circuit in Fig. 1 during a switching cycle, whereas Fig. 4 shows its key waveforms. It should be noted that because the junction capacitance of boost rectifier D is neglected in this analysis, clamp diode D_C is not shown in Fig. 3 since it never conducts.

As can be seen from the timing diagrams for the boost and auxiliary switches in Fig. 4, the switches never conduct simultaneously. In fact, the proper operation of the power stage, *i.e.*, the operation which reduces reverse-recovery related losses and enables soft switching, requires appropriate dead times between the turn-off of boost switch S and turn-on of auxiliary switch S_1 , and vice versa. Before main switch S is turned off at $t = T_0$, the entire input current, I_{in} , flows through inductor L_S and switch S . At the same time, rectifier D is off with a reverse voltage across its terminals equal to output voltage V_O . Auxiliary switch S_1 is also off, blocking the voltage $V_O - V_C$, where V_C is the voltage across clamp capacitor C_C .

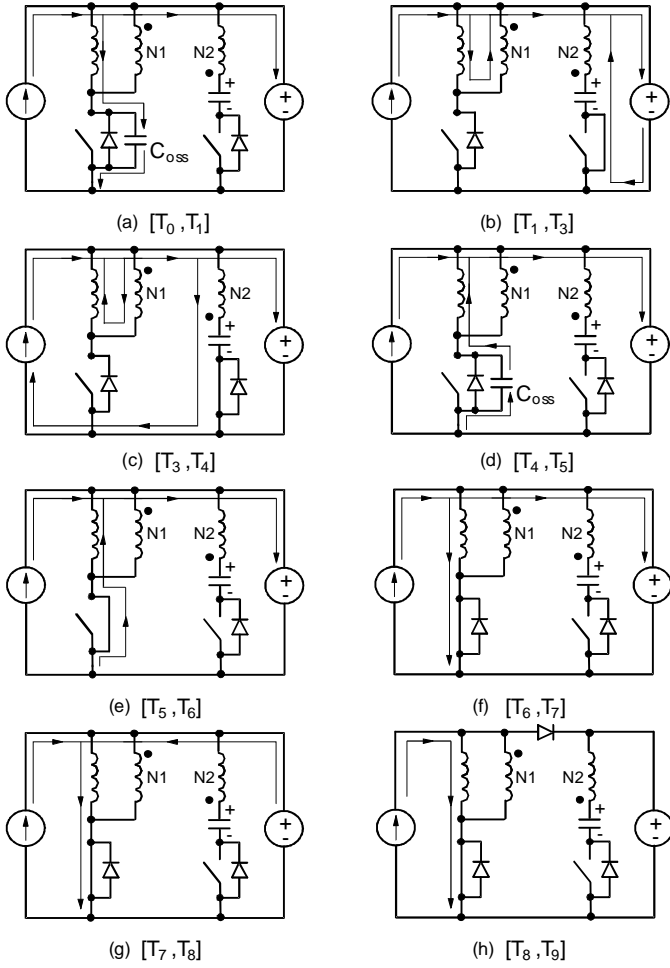


Fig. 3 Topological stages of the proposed boost power stage.

After switch S is turned off at $t = T_0$, the current which was flowing through the channel of the MOSFET of switch S is diverted to the output capacitance of the switch, C_{oss} , as shown in Fig. 3(a). As a result, the voltage across switch S starts to increase linearly due to the constant charging current I_{in} . At the same time, voltage V_D across boost rectifier D starts decreasing toward zero. Since during the time interval rectifier voltage V_D decreases from V_O to zero, the voltage across inductor L_S is zero (due to constant current I_{in}), auxiliary-switch voltage v_{S1} stays constant at $V_O - V_C$. When voltage across switch S reaches V_O , rectifier D starts conducting, as shown in Fig. 3(a). After D starts conducting, auxiliary-switch voltage v_{S1} starts decreasing from $V_O - V_C$ toward zero. Because inductor current i_{LS} continues to charge C_{oss} after v_S reaches V_O , v_S continues to increase above V_O , causing the current through inductor L_S to start decreasing due to a negative voltage across its terminals, as shown in Fig. 4. This topological stage ends at $t = T_1$, when voltage v_{S1} reaches zero, *i.e.*, when the antiparallel diode of switch S_1

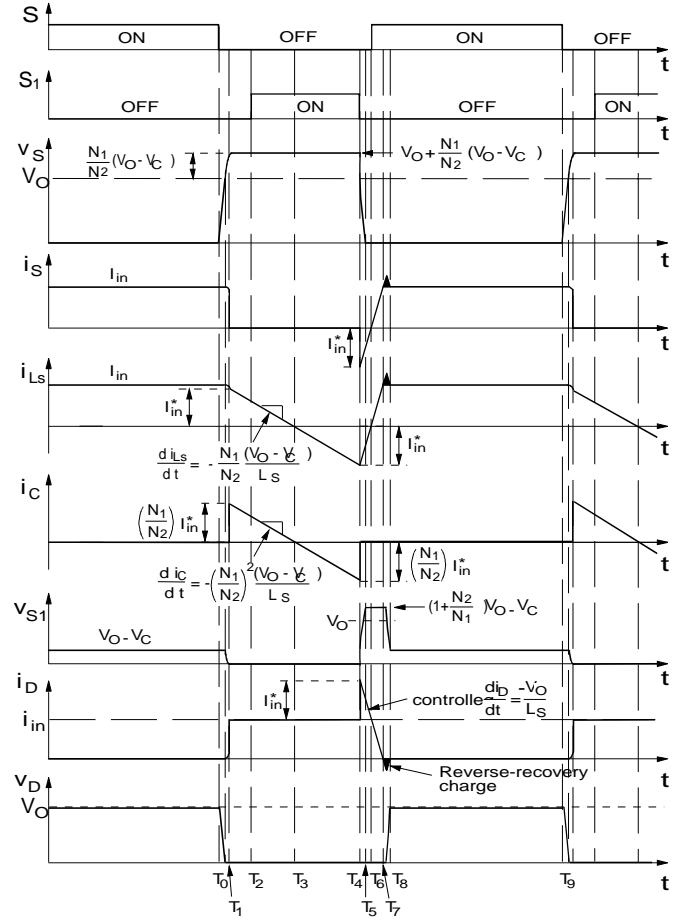


Fig. 4 Key waveforms of the proposed boost power stage.

starts conducting. At that moment, the remaining inductor current i_{LS} is diverted into clamp capacitor C_C through the magnetic coupling of windings N_1 and N_2 , as shown in Fig. 3(b). During the time intervals the clamp-capacitor current flows, its magnitude is given by $i_C = (N_1/N_2)i_{LS} = ni_{LS}$, *i.e.*, it is proportional to snubber-inductor current i_{LS} . Also, at $t = T_1$ main-switch voltage v_S reaches its maximum equal to $V_O + (N_1/N_2)(V_O - V_C)$, as shown in Fig. 4.

During the topological stage shown in Fig. 3(b), inductor current i_{LS} continues to decrease as the energy stored in L_S continues to be transferred into clamp capacitor C_C (Fig. 4). If the capacitance of C_C is large, capacitor voltage V_C is almost constant, and inductor current i_{LS} as well as capacitor current i_C decrease linearly. Otherwise, i_{LS} and i_C decrease in a resonant fashion. This topological stage ends at $t = T_3$, when i_C reaches zero, and the antiparallel diode of auxiliary switch S_1 stops conducting. To achieve ZVS of S_1 , it is necessary to turn on the transistor of switch S_1 before $t = T_3$, *i.e.*, while its antiparallel diode is conducting. In Fig. 4, the MOSFET of switch S_1 is turned on at $t = T_2$.

If the transistor of switch S_1 is turned on prior to $t = T_3$, inductor current i_{L_S} will continue to flow after $t = T_3$ in the opposite direction through the closed transistor of switch S_1 , as shown in Fig. 3(c). During this topological stage, the energy stored in clamp capacitor C_C during interval $[T_1 - T_3]$ is returned to the inductor in the opposite direction. This interval ends at $t = T_4$ when auxiliary switch S_1 is turned off.

When, at $t = T_4$, S_1 is turned off, clamp-capacitor current i_C stops flowing. Because the current through winding N_2 is $i_C = 0$, the reflected current into winding N_1 is also zero, and i_{L_S} is forced to flow through output capacitance C_{OSS} of boost switch S , as shown in Fig. 3(d). Also, at $t = T_4$, the voltage of auxiliary switch S_1 and boost-rectifier current i_D abruptly increase from zero to $V_O - V_C$, and from I_{in} to $I_{in} + I_{in}^*$, respectively. Since in this topological stage i_{L_S} discharges C_{OSS} , boost-switch voltage v_S decreases from $V_O + (N_1/N_2)(V_O - V_C)$ towards zero. At the same time, i_{L_S} increases toward zero and i_D decreases toward I_{in} , as shown in Fig. 4.

Whether v_S will decrease all the way to zero depends on the energy stored in inductor L_S at $t = T_4$. If this energy is larger than the energy required to discharge C_{OSS} from $V_O + (N_1/N_2)(V_O - V_C)$ down to zero, *i.e.*, if

$$\frac{1}{2} L_S [i_{L_S}(t = T_4)]^2 \geq \frac{1}{2} C_{OSS} |V_O + \frac{N_1}{N_2} (V_O - V_C)|^2, \quad (1)$$

then v_S will reach zero. Otherwise, v_S will not be able to fall to zero, and will tend to oscillate around the V_O level if boost switch S is not turned on immediately after v_S reaches its minimum.

Assuming that inductor energy is more than enough to discharge C_{OSS} to zero, v_S will reach zero at $t = T_5$, while inductor current i_{L_S} is still negative. As a result, the antiparallel diode of S will start conducting as shown in Fig. 3(e). Because of the simultaneous conduction of the antiparallel diode of S and rectifier D , constant output voltage V_O is applied to inductor L_S so that inductor current i_{L_S} increases linearly toward zero (Fig. 4). To achieve ZVS of switch S , it is necessary to turn on the transistor of switch S during the time interval $[T_5 - T_6]$, when the antiparallel diode of S is conducting. If the transistor of S is turned on during this interval, i_{L_S} will continue to increase linearly after $t = T_6$, as shown in Fig. 3(f). At the same time, rectifier current i_D will continue to decrease linearly. The rate of the i_D decrease is determined by the value of L_S inductance because

$$\frac{di_D}{dt} = -\frac{V_O}{L_S}. \quad (2)$$

To reduce the rectifier-recovered charge and the associated losses, a proper L_S inductance needs to be selected [6]. Generally, a larger inductance, which gives a lower di_D/dt

rate, results in a more efficient reduction of the reverse-recovery-associated losses [1].

The linear increase of i_{L_S} should stop at $t = T_7$, when i_{L_S} reaches the input-current level I_{in} , and rectifier current i_D falls to zero (Fig. 4). However, due to the residual stored charge, rectifier current i_D starts flowing in the reverse direction, as shown in Fig. 3(g), producing an overshoot of the switch current over the I_{in} level, as shown in Fig. 4. Without L_S , this reverse-recovery current would be many times larger. Once the rectifier has recovered at $t = T_8$, the entire input current I_{in} flows through switch S (Fig. 3(h)), until the next switching cycle is initiated at $t = T_9$.

Besides the stored charge that needs to be recovered before fast-recovery rectifier D can block voltage, the rectifier possesses a junction capacitance. This junction capacitance was neglected in the previous analysis of operation. However, in a practical boost circuit, this capacitance interacts with the snubber inductance causing an undesirable parasitic ringing of the rectifier voltage after the rectifier has recovered. This ringing significantly increases the voltage stress of the rectifier [6]. As explained in [7], the ringing can be completely eliminated by the addition of diode D_C , shown in Fig. 1. With clamp diode D_C , the voltage stress of boost rectifier D in the proposed circuit is the same as in the conventional, "hard"-switched converter, *i.e.*, it is equal to V_O .

III. Design Considerations

As explained earlier, to achieve ZVS of main switch S , it is necessary that the energy stored in L_S at the moment auxiliary switch S_1 is turned off be larger than or equal to the energy required to discharge output capacitance C_{OSS} of switch S from $V_O + (N_1/N_2)(V_O - V_C)$ down to zero. Since the energy stored in L_S is proportional to the square of the output (load) current, it is easier to satisfy the ZVS condition in Eq. (1) at heavier loads than at lighter loads. As a result, at light loads switch S does not operate with ZVS. On the other hand, auxiliary switch S_1 operates with ZVS in virtually the entire load range, because it uses energy stored in boost inductor L , which is much larger than that stored in snubber inductor L_S , to discharge its output capacitance.

To reduce the reverse-recovery-related losses, the di/dt rate of the majority of today's fast-recovery rectifiers should be kept below approximately 100 A/ μ s [1]. Generally, slower rectifiers require slower di/dt rates than faster rectifiers to achieve the same level of reduction of the reverse-recovery-related losses. As a rule of thumb, the practical range of snubber inductance L_S is from 2 μ H to 20 μ H.

As can be seen from Fig. 4, the voltage stress of main switch S is $V_O + (N_1/N_2)(V_O - V_C)$, whereas the stress of auxiliary switch S_1 is $(1 + N_2/N_1)V_O - V_C$. Therefore, the voltage stress of main switch S in the proposed converter is

higher for the amount of $(N_1/N_2)(V_O - V_C)$ compared to the corresponding stress in the conventional, “hard”-switched boost converter. To keep the voltage stress of switches S and S_1 within reasonable limits, it is necessary to properly select clamp-voltage level V_C .

From Fig. 4, it can be seen that from $t = T_1$ to $t = T_3$ clamp capacitor C_C is discharged with current i_C which has a constant slope of $di_C/dt = (N_1/N_2)^2(V_O - V_C)/L_S$. Therefore, since $i_C(t = T_1) = (N_1/N_2)i_{LS}(t = T_1) = (N_1/N_2)I_{in}^* \approx (N_1/N_2)I_{in}$, and since the duration of the time interval $[T_1 - T_3]$ is approximately one-half of the off-time of main switch S, clamp-capacitor voltage V_C , can be expressed as

$$V_C = V_O - L_S \frac{(N_2/N_1)I_{in}}{(1-D)T_S/2} = V_O - 2 \left| \frac{N_2}{N_1} \right| \frac{L_S f_S I_{in}}{1-D}, \quad (3)$$

where D is the duty-cycle of switch S, T_S is the switching period, and f_S is the switching frequency. Since for a lossless boost power stage,

$$\frac{V_O}{V_{in}} = \frac{I_{in}}{I_O} = \frac{1}{1-D}, \quad (4)$$

Eq. (3) can be written as

$$V_O - V_C = 2 \left| \frac{N_2}{N_1} \right| L_S f_S I_O \left(\frac{V_O}{V_{in}} \right)^2. \quad (5)$$

According to Eq. (5), $V_O - V_C$ is maximum at full load $I_{O(max)}$ and low line $V_{in(min)}$. For given input and output specifications, *i.e.*, for given $I_{O(max)}$, $V_{in(min)}$, and V_O , the voltage stresses on the main and auxiliary switches can be minimized by minimizing the $(N_2/N_1)L_S f_S$ product.

It should be noted that the leakage inductance of the inductor in Fig. 1 needs to be minimized since it resonates with the output capacitance of boost switch S and auxiliary switch S_1 after the switches are turned off at $t = T_0$ and $t = T_4$, respectively. If the leakage inductance is excessive, the parasitic resonances can increase significantly the voltage stress of the switches. The leakage inductance of the coupled inductor can be minimized by using the bifilar winding technique. It should be noted that the energy contained in these parasitic resonances is much lower than the rated avalanche energy of today’s MOSFETs. Consequently, these parasitic resonances do not cause a device failure even if the peak voltage of the resonances is clamped by the breakdown voltage of the devices. However, the resonances might have a more dramatic effect on the EMI performance.

In input-current-shaping applications, the circuit in Fig. 1 needs an additional rectifier to prevent the voltage across clamp capacitor C_C from exceeding V_O . Namely, due to the varying line voltage and constant output voltage, the duty cycle of the boost-converter input-current shaper varies. It is

close to 100% around the zero crossings of the line voltage, and it is smallest at the peak of the line voltage. When the line voltage is around zero, the energy stored in the boost inductor is small even with the switch duty cycle close to 100%. As a result, after switch S in Fig. 1 is turned off, the inductor stored energy is not sufficient to charge output capacitance C_{OSS} of S up to $V_O + V_C$, and force the conduction of the antiparallel diode of auxiliary switch S_1 . Since around zero crossings of the line voltage antiparallel diode of S_1 does not conduct, the auxiliary switch does not turn on at zero voltage and, consequently, capacitor C_C does not discharge. However, every time the MOSFET of S_1 is turned on, clamp capacitor C_C is charged for a brief duration of switch S_1 conduction. Since around line-voltage zero crossings, C_C is only charged, clamp capacitor voltage V_C will increase. If V_C exceeds V_O , no reset voltage for the core of the coupled inductor will be available, and the core would saturate. To prevent V_C from exceeding V_O , clamp diode D_{C1} should be added to the active clamp as shown in Fig. 5.

Finally, it should be noted that the control of the proposed boost converter can be implemented in the same way as in its conventional “hard” switched counterpart as long as an additional gate-driver circuit is provided. Specifically, in the input-current-shaping applications, the proposed converter can be implemented with any known control technique such as average current, peak current, or hysteretic control.

IV. Experimental Results

The performance of the boost converter with the isolated active snubber was evaluated on a 1 kW (375 V/ 2.67 A), universal-line-voltage (90 - 265 V_{ac}) power-factor-correction circuit operating at 80 kHz. The component values of the experimental circuit are shown in Fig. 5.

Boost inductor L was built using Magnetics toroidal core Kool Mu 77439-A7 (two cores in parallel) and 55 turns of AWG#14, whereas snubber inductor L_S was built with Magnetics toroidal core MPP 55550-A2 (two cores in parallel) with $N_1 = N_2 = 9$ bifilarly wound turns of AWG#14. The measured leakage inductance of L_S was 250 nH. The control circuit was implemented with the average-current PFC controller UC3854. The TC4420 and TSC429 drivers are used to generate the required gate-drive signals for the main and auxiliary switches, respectively.

With the selection of $L_S = 4.7 \mu\text{H}$, the di/dt turn-off rate of the rectifier was limited to $di/dt = V_O/L_S = 80 \text{ A}/\mu\text{s}$. In addition, the minimum voltage of clamp capacitor C_C , which occurs at the minimum line voltage and full load, was limited to approximately 325 V. With $V_{C(min)} = 325 \text{ V}$, the maximum voltage stresses on the switches were limited to $2V_O - V_{C(min)} = 425 \text{ V}$.

Figure 6 shows the gate-drives, main-switch drain-to-source, and boost rectifier voltage waveforms of the

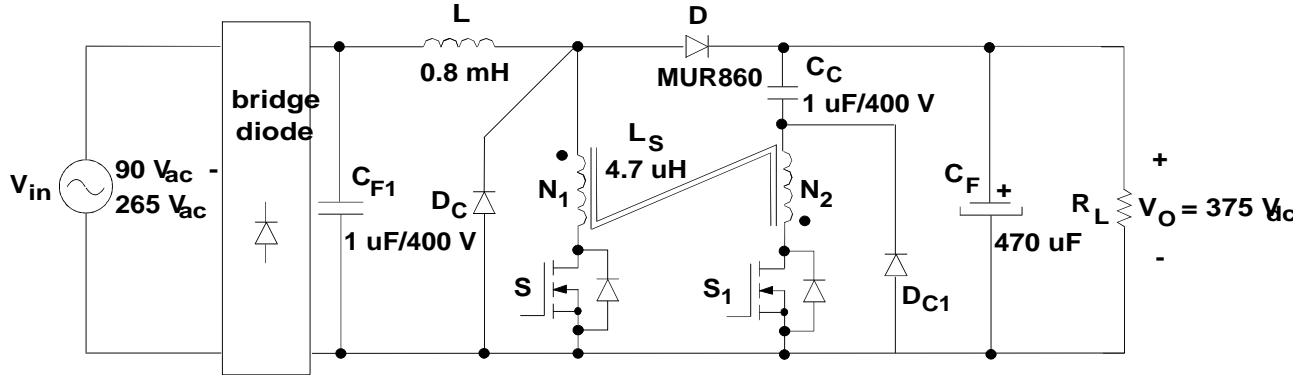


Fig. 5 Experimental 1 kW, universal-input-voltage boost power stage with isolated active-clamp snubber.

experimental converter operating at the minimum line ($V_{in}^{\min} = 90 V_{ac}$) and full power of 1 kW. As can be seen from Fig. 6(a), the voltage stress on the main switch is less than 425 V, whereas the maximum boost-rectifier reverse voltage is 375 V, *i.e.*, it is equal to output voltage V_O . Also, from Fig. 6(b), which shows an enlarged turn-on transition of the waveforms in Fig. 6(a), it can be seen that boost switch S turns on when the voltage across it is zero. As a result of the zero-voltage switching of S , its turn-on output-capacitance discharge loss is eliminated. For $L_S = 4.7 \mu H$, the experimental converter can operate with zero-voltage switching down to 30% of the full load at the minimum line voltage.

Figure 7 shows the measured efficiencies of the experimental converter with (solid lines) and without (dashed lines) the isolated active snubber at the minimum and maximum line voltages as functions of the output power. As can be seen from Fig. 7, for both line voltages the active snubber improves the conversion efficiency in the entire measured power range (300 W to 1 kW). Nevertheless, the efficiency improvement is more pronounced at the minimum line and higher power levels where the reverse-recovery losses are greater. Specifically, at the maximum line (265 V_{ac}), the efficiency improvement at 1 kW is 0.3%. However, at the minimum line, the implementation without the active snubber cannot deliver more than approximately 700 W due to the thermal runaway of the diode caused by excessive reverse-recovery losses. At $P_O = 700$ W, the active snubber improves the efficiency by approximately 3%, which translates into approximately 30% reduction of the losses.

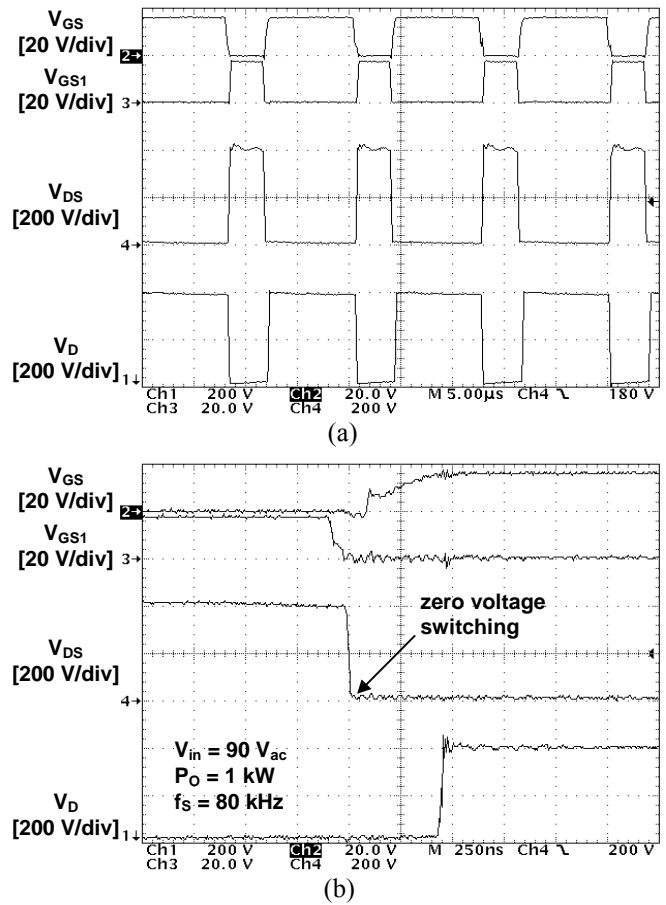


Fig. 6 Oscilloscope waveforms of gate-drive voltages V_{GS} and V_{GS1} , boost-switch drain-to-source voltage V_{DS} , and boost rectifier voltage V_D waveforms at low line (90 V_{ac}) and full power (1 kW): (a) 5 μs time base; (b) 250 ns time base.

Furthermore, at the same power levels, the temperatures of the semiconductor components in the implementation with the active snubber are significantly lower than those in the implementation without the snubber. As indicated in Fig. 7, at

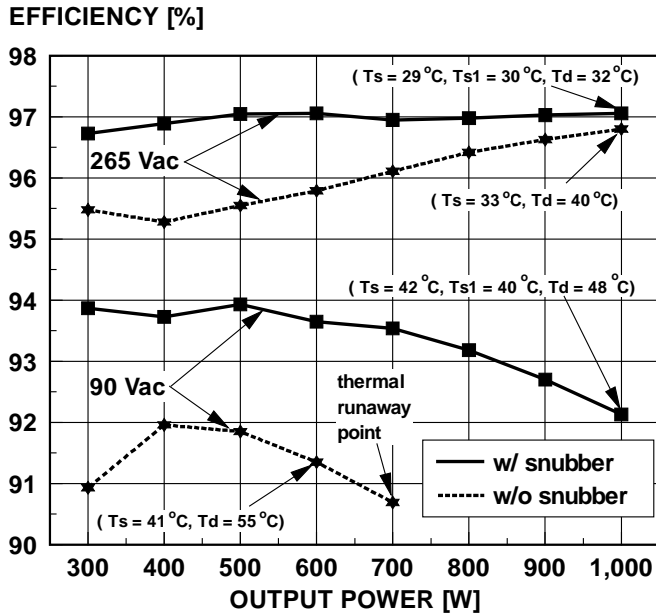


Fig. 7 Measured, full-power efficiencies of the experimental converter with (solid lines) and without (dashed lines) isolated active snubber at the minimum and maximum line voltages as functions of the output power. Note that the maximum possible output power for the implementation without the snubber is limited to 700 W.

the maximum line (265 V_{ac}) and full power (1 kW), the case temperatures of the boost rectifier and boost switch in the implementation with the snubber are $T_d = 32^\circ\text{C}$ and $T_s = 29^\circ\text{C}$, respectively, whereas the corresponding temperatures in the implementation without the snubber are $T_d = 40^\circ\text{C}$ and $T_s = 33^\circ\text{C}$. Similarly, at the minimum line voltage (90 V_{ac}) and full power, the rectifier and switch temperatures in the implementation with the snubber are $T_d = 48^\circ\text{C}$ and $T_s = 42^\circ\text{C}$. As can be seen from Fig. 7, the implementation without the snubber cannot deliver the full power of 1 kW at the minimum line because the rectifier becomes thermally unstable at approximately 700 W. In fact, for the implementation without the snubber the temperature of the boost rectifier is $T_d = 55^\circ\text{C}$ at 600 W, which is significantly higher than the temperature of the rectifier ($T_d = 48^\circ\text{C}$) in the implementation with the snubber at 1 kW.

V. Summary

An active-snubber technique which reduces the reverse-recovery-related losses and reduces the capacitive-discharge turn-on switching loss of the boost converter is described. The snubber consists of a coupled inductor, clamp-capacitor, and ground-referenced, N-channel MOSFET. The operation and performance of the proposed technique was verified on an 1 kW, universal-line-voltage boost input-current shaper. The results of the experimental evaluation have shown that the proposed active-snubber technique can significantly extend the maximum power range at which a fast-recovery rectifier can be reliably applied.

References

- [1] Y. Khersonsky, M. Robinson, D. Gutierrez, "New fast recovery diode technology cuts circuit losses, improves reliability," *Power Conversion & Intelligent Motion (PCIM) Magazine*, pp. 16 - 25, May 1992.
- [2] R. Streit, D. Tollik, "High efficiency telecom rectifier using a novel soft-switched boost-based input current shaper," *International Telecommunication Energy Conf. (INTELEC) Proc.*, pp. 720 - 726, Oct. 1991.
- [3] G. Hua, C.S. Leu, F.C. Lee, "Novel zero-voltage-transition PWM converters," *IEEE Power Electronics Specialists' Conf. (PESC) Rec.*, pp. 55 - 61, June 1992.
- [4] D.C. Martins, F.J.M. de Seixas, J.A. Brilhante, I. Barbi, "A family of dc-to-dc PWM converters using a new ZVS commutation cell," *IEEE Power Electronics Specialists' Conf. (PESC) Rec.*, pp. 524 - 530, June 1993.
- [5] J. Bassett, "New, zero voltage switching, high frequency boost converter topology for power factor correction," *International Telecommunication Energy Conf. (INTELEC) Proc.*, pp. 813 - 820, Oct. 1995.
- [6] C.M.C. Duarte, I. Barbi, "A new family of ZVS-PWM active-clamping dc-to-dc boost converters: analysis, design, and experimentation," *International Telecommunication Energy Conf. (INTELEC) Proc.*, pp. 305 - 312, Oct. 1996.
- [7] M.M. Jovanović, "A technique for reducing rectifier reverse-recovery-related losses in high-voltage, high-power boost converters," *IEEE Applied Power Electronics (APEC) Conf. Proc.*, pp. 1000 - 1007, Mar. 1997.
- [8] K. Harada, H. Sakamoto, "Switched snubber for high frequency switching," *IEEE Power Electronics Specialists' Conf. (PESC) Rec.*, pp. 181 - 188, June 1990.